Title

Technical note with Supporting Results forOutlier Accommodation Nonlinear State Estimation:A Risk-Averse Performance-Specified Approach

Authors

Aghapour, Elahe
Rahman, Farzana
Farrell, Jay

Publication Date

2019-06-25

Technical note with Supporting Results for Outlier Accommodation Nonlinear State Estimation: A Risk-Averse Performance-Specified Approach

Elahe Aghapour, Farzana Rahman, Jay A. Farrell
Department of Electrical and Computer Engineering,
University of California, Riverside, 92521.
{eaghapour, frimi, farrell}@ee.ucr.edu.

This tech note extends and supports the results in [1]. The main article should be read first. That article presents RAPS for nonlinear applications.

This technical note has two main parts. Section I presents the derivation (related to Section VI-B in [1]) for choosing the lower bound J_l in vehicle state estimation applications. Section II presents a linear position, velocity, and acceleration (PVA) vehicle model and experimental results using the same GPS data as used in the main article. The linear system RAPS application is a special case of the appraoch presented in [1]. The numerical results specific linear systems did not fit within the journal page constraints. The linear application is referred to in the GNSS literature as a PVA model wherein the GNSS measurements are used to estimate the position, velocity, and acceleration of the GNSS antenna. Such estimators are included in almost all GNSS receivers.

I. Choosing J_l For Vehicle State Estimation

In highway vehicle applications horizontal position accuracy is of primary importance. In particular, the SAE specification [2] requires 1.5 meter horizontal position accuracy with 68% probability.

If the first two elements of the state vector are the north and east components of position and their error is distributed as $w = [\delta x_1, \delta x_2]^\top \sim \mathcal{N}(0, P_h)$, the probability density is:

$$p(\delta x_1, \delta x_2) = \frac{1}{2\pi |P_h|^{0.5}} exp\Big(-\frac{1}{2} w^\top P_h^{-1} w\Big).$$

where $|A|$ denotes the determinant of matrix A. Since P_h is symmetric positive definite, there is an unitary matrix U and positive definite matrix $\Sigma = diag(\sigma_1, \sigma_2)$ such that $P_h = U\Sigma^2 U^\top$.

For the analysis, consider the two random variables $v = Sw$ and $y = U^\top w$ where $S = \Sigma^{-1} U^\top$. Then, $v \sim \mathcal{N}(0, I)$ and $y \sim \mathcal{N}(0, \Sigma^2)$. The probability density function for v is:

$$p(v) = \frac{1}{2\pi} exp\Big(-\frac{1}{2} v^\top v\Big).$$

For scalars $0 \le \beta \le 1$ and $c \ge 0$, define

$$\beta = Prob\{\|v\| \le c\}. \tag{1}$$

The random variable $\rho = \|v\|$ is a Rayleigh random variable (see Section 4.9.1.2 in [3]) with distribution

$$P_\rho(r) = 1 - exp\left(-\frac{r^2}{2}\right).$$

Therefore, given a value for β, selecting c to satisfy

$$\beta = 1 - exp\left(-\frac{c^2}{2}\right) \tag{2}$$

(e.g., $\beta = 68\%$ yields $c = 0.99$) results in eqn. (1) being satisfied.

For the definitions of v and y, eqn. (1) is equivalent to:

$$\begin{aligned}
\beta &= Prob\{\|v\| \le c\} \\
&= Prob\{w^\top S^\top S w \le c^2\} \\
&= Prob\{w^\top P_h^{-1} w \le c^2\} \qquad = Prob\{\|w\|_P^2 \le c^2\} \\
&= Prob\{y^\top U P_h^{-1} U^\top y \le c^2\} \\
&= Prob\{y^\top \Sigma^{-2} y \le c^2\} \qquad = Prob\{\|y\|_{\Sigma^2}^2 \le c^2\}.
\end{aligned}$$

These expressions use the Mahalonobis norm defined as $\|x\|_Q^2 = x^\top Q^{-1} x$, which arises naturally when working with normal distributions. For the choice of c from eqn. (2)

$$\beta = Prob\{\|w\|_P^2 \le c^2\} = Prob\{\|y\|_{\Sigma^2}^2 \le c^2\}.$$

The regions

$$\|w\|_P^2 \le c^2 \quad \text{and} \tag{3}$$

$$\|y\|_{\Sigma^2}^2 = \frac{\delta y_1^2}{\sigma_1^2} + \frac{\delta y_2^2}{\sigma_2^2} \le c^2 \tag{4}$$

each defines an ellipse. The region $\|w\| \le c$ defines a circle. Eqn. (4) shows that

$$\frac{1}{\overline{\sigma}} \|y\| \le \|y\|_{\Sigma^2} \le \frac{1}{\underline{\sigma}} \|y\|,$$

where $\overline{\sigma} = \max(\sigma_1, \sigma_2)$ and $\underline{\sigma} = \min(\sigma_1, \sigma_2)$. The fact that U is unitary implies that $\|w\| = \|y\|$ and $\|w\|_P = \|y\|_{\Sigma^2}$ by the definition of y, so that

$$\frac{1}{\overline{\sigma}} \|w\| \le \|w\|_P \le \frac{1}{\underline{\sigma}} \|w\|.$$

Therefore, the circle $\|w\| \le c\overline{\sigma}$ contains the ellipse $\|w\|_{P^{-1}} \le c$. Therefore,

$$Prob\{\|w\|^2 < \overline{\sigma}^2 c^2\} \quad \ge \quad Prob\{\|w\|_{P^{-1}}^2 < c^2\} = \beta.$$

To satisfy the requirement that $\|w\| \leq R|_{R=1.5m}$ with at least $\beta = 68\%$ probability, requires[1]:

$$P_h \leq \varepsilon^2 I$$

where $\varepsilon = \frac{R}{c} = \frac{1.5}{0.99}$ and I is the identity in two dimensions. This inequality ensure that $\overline{\sigma} \leq \varepsilon$. By the analysis above:

$$\begin{aligned} Prob\{\|w\| < 1.5\} &= Prob\{\|w\|^2 < \varepsilon^2 c^2\} \\ &\geq Prob\{\|w\|^2_{P^{-1}} < c^2\} = \beta = 68\%. \end{aligned}$$

Therefore, the upper bound on the covariance is $P_u = \varepsilon^2 I$. The lower bound on the information matrix is $J_l = \frac{1}{\varepsilon^2} I$.

II. Linear PVA Results

A. Linear (PVA) Model

The rover state is $x = [p^\top, v^\top, a^\top]^\top \in \mathbb{R}^9$ where p, v and $a \in \mathbb{R}^3$ represent the rover position, velocity and acceleration vectors, respectively. The three vectors that comprise x are each represented in local tangent frame coordinates such that the position vector has north, east, and down elements (in that order). Therefore, the horizontal position accuracy is determined by the accuracy of the first two components of x.

The continuous-time PVA vehicle model is

$$\dot{x}(t) = \begin{bmatrix} 0 & I & 0 \\ 0 & 0 & I \\ 0 & 0 & -\lambda_a I \end{bmatrix} x(t) + \begin{bmatrix} 0 \\ 0 \\ I \end{bmatrix} \omega_a(t),$$

where I is the identity matrix in $\mathbb{R}^3$ and $\omega_a(t)$ is modeled as Gaussian white noise with independent elements each with power spectral density $Q_a = \sigma_a^2$.

The corresponding PVA discrete-time propagation model is

$$x_k = \Psi_{k-1} x_{k-1} + G_{k-1} u_{k-1} + \omega_{k-1}. \tag{5}$$

with

$$\psi_k = \begin{bmatrix} I & TI & a_3 I \\ 0 & I & a_2 I \\ 0 & 0 & a_1 I \end{bmatrix}, \Gamma_k \approx \begin{bmatrix} T^{5/2}/\sqrt{20} I \\ T^{3/2}/\sqrt{3} I \\ \sqrt{T} I \end{bmatrix}, \text{ and } Q_d = \begin{bmatrix} 0 \\ 0 \\ \sigma_a^2 I \end{bmatrix},$$

where all submatrices are three by three with $a_1 = e^{-\lambda_a T}$,

$$a_2 = \left(1 - e^{-\lambda_a T}\right)/\lambda_a, \qquad a_3 = \left(\lambda_a T - 1 + e^{-\lambda_a T}\right)/\lambda_a^2$$

and $\omega_k \sim \mathcal{N}(0, Q_d)$ where Q_d is a covariance matrix. The approximation indicated in Γ_k yields the correct diagonal of the discrete-time noise covariance matrix, but $\Gamma_k Q_d \Gamma_k^\top$ approximates the off-diagonal terms relative to the exact calculation. The details of the model and its parameters are in [4].

The state estimation is updated using double-differenced GNSS pseudorange and Doppler measurements using the models in Section VII-A in [1].

B. Performance Specification

For the results herein, only the performance of the horizontal position was constrained in the RAPS optimization.

[1]The inequality is interpretted in the matrix sense:

$$A \leq B \quad \leftrightarrow \quad x^\top A x \leq x^\top B x$$

for all $x \neq 0$.

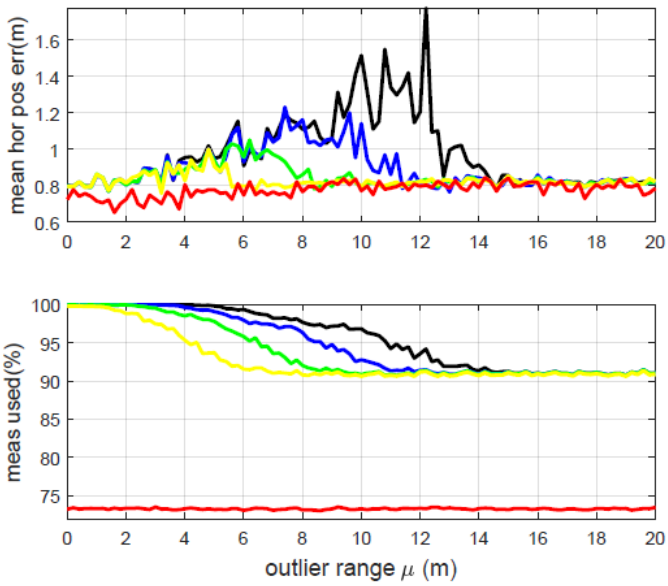

Fig. 1: Mean horizontal position error and the percentage of selected measurements versus mean outlier magnitude $\mu \in [0, 20]$. The red curves display the result for the binary RAPS algorithm. The yellow, green, blue and black curves show the results for the NP-(E)KF approach with γ=2, 3, 4, and 5, respectively.

C. Experimental Results

Each table and figure herein considers five algorithms, as summarized in Section IX-B of [1]. Four of the algorithms are the NP-KF with four different values of the decision parameter γ. The final algorithm is the RAPS approach. The error, risk and PVA metrics are defined in Section IX-C and IX-E of [1].

Fig. 1 shows NP-KF and RAPS state estimation accuracy as characterized by horizontal position error. As explained in Section IX-D in [1], for each value of $\mu \in [0, 20]$ meter, each point on each curve is produced as the average of horizontal position error over 300 seconds and 10 Monte Carlo experiments. For each Monte Carlo run, the same outlier corrupted data is used for all NP-KF and RAPS algorithms. The x-axis in both sub-figures is the mean outlier magnitude. The y-axis in the top sub-figure is the mean of the horizontal position error. The y-axis in the bottom sub-figure is the percentage of measurements used by the state estimation algorithm. At each time instant, the measurement set (pseudorange and Doppler) contains 9% generated outliers. Fig. 1 shows the NP-KF mean horizontal position error initially increases and later falls as the magnitude of the outlier increases. The initial rise is due to small outliers being likely to pass through the threshold test. As the magnitude of the outlier (i.e., μ) increases, each NP threshold test removes an increasingly higher percentage of the outliers, until it is correctly removing all the measurements which are affected by outliers. Correct rejection of all outliers occurs for smaller values of μ as the NP threshold γ decreases. The RAPS mean horizontal error is always less than that for NP-KF, regardless of the value of the threshold γ. This shows that the RAPS approach is robust to the magnitude of the outlier, without the designer having to pick a value for a test parameter (e.g., the NP threshold γ).

Fig. 2 presents graphs of the horizontal error (top), risk

R_k (middle) and GDOP (bottom) for a portion of a single experiment using the GNSS data with the linear PVA model. The computation of R_k and GDOP is explained in Section IX-E of [1]. The algorithm cooresponding to each curve is defined in the figure caption. The five algorithms are explained in Section IX-B of [1]. Fig. 2 allows performance comparisons between the five algorithms for two different values of the outlier mean magnitude μ. Fig. 2a presents data for $\mu = 6$ (i.e. outliers magnitude distributed in $U[4.5, 7.5]$). Fig. 2b presents data for $\mu = 17$ (i.e. outliers magnitude distributed in $U[15.5, 18.5]$).

For $\mu = 6$, RAPS both achieves the minimum risk at all times and the best horizontal position accuracy at most times. The lowest risk is expected as RAPS minimizes risk. The best positioning performance is less obvious, especially as the GDOP of RAPS is highest, because it uses fewer measurements. A reason why RAPS achieves the best positioning performance is due to its having the lowest risk of outlier inclusion. For any of the algorithms, once an outlier is included, then both the prior mean and covariance are wrong, which affects the validity of all subsequent state estimation and decision making about which measurements to use. Minimizing the risk of outlier inclusion therefore has benefits for both accuracy and reliability, especially when there are more measurements available than are required to meet a stated specification.

The performance of NP-KFs improves for $\mu = 17$ relative to the case where $\mu = 6$. This is because outliers with larger magnitude are more likely to be detected for any fixed value of the decision parameter γ. When all the algorithms correctly remove the outliers, their curves are overlapping. RAPS performance is almost the same for both scenarios, because it considers all feasible solutions and selects the one with minimum risk. Hence, its error is robust for different values of μ.

Tables Ia and Ib provide vertical and horizontal positioning accuracy statistics, respectively, for the five linear estimation algorithms using the PVA model. In both Tables, the top section is for $\mu = 6$ and the bottom sections is for $\mu = 17$. In all statistics, the RAPS algorithm performance is the best.

REFERENCES

[1] E. Aghapour, F. Rahman, and J. A. Farrell, "Outlier accommodation in state estimation: A risk-averse performance-specified approach," *Submitted to IEEE T. on Control Systems Technology*, October 2018.

[2] Anonymous, "On-Board System Requirements for V2V Safety Communications," SAE, Tech. Rep., March, 2016. [Online]. Available: https://saemobilus.sae.org/content/j2945/1_201603

[3] J. Farrell, *Aided Navigation: GPS with High Rate Sensors*. McGraw-Hill, Inc., 2008.

[4] F. Rahman, E. Aghapour, and J. A. Farrell, "ECEF Position Accuracy and Reliability in the Presence of Differential Correction Latency Year 1 Technical Report for Sirius XM," UCR, Tech. Rep., October, 2018. [Online]. Available: escholarship.org/uc/item/38d3h08w

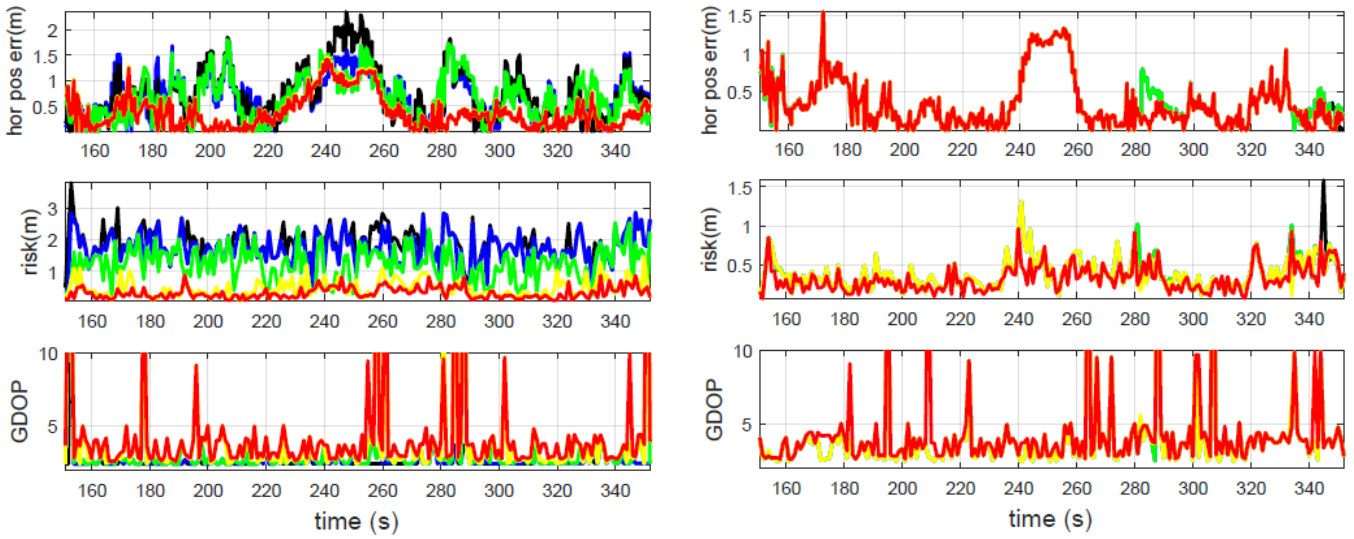

(a) Horizontal Position Error, Risk, and GDOP for $\mu = 6$

(b) Horizontal Position Error, Risk, and GDOP for $\mu = 17$

Fig. 2: Performance comparison using GNSS data with the linear PVA model. The yellow, green, blue and black curves display the results for NP-KF approach γ=2, 3, 4, and 5, respectively. The red curve shows the RAPS performance.

TABLE I: GNSS-PVA Performance Statistics

(a) Vertical: $\mu = 6$ (top) and $\mu = 17$ (bottom).

Methods	Mean of error (m)	Std. of error (m)	Error < 2 m	Maximum error (m)
NP-KF1 $\gamma = 5$	2.85	0.76	0.12	5.04
NP-KF1 $\gamma = 4$	2.82	0.74	0.10	5.02
NP-KF1 $\gamma = 3$	2.20	0.83	0.38	4.11
NP-KF1 $\gamma = 2$	0.68	0.60	0.96	3.30
RAPS1	0.56	0.46	0.99	2.07
NP-KF1 $\gamma = 5$	0.55	0.48	0.99	2.39
NP-KF1 $\gamma = 4$	0.55	0.48	0.99	2.39
NP-KF1 $\gamma = 3$	0.55	0.48	0.99	2.39
NP-KF1 $\gamma = 2$	0.55	0.48	0.99	2.40
RAPS2	0.56	0.46	0.99	2.09

(b) Horizontal: $\mu = 6$ (top) and $\mu = 17$ (bottom).

Methods	Mean of error (m)	Std. of error (m)	Sub-meter accuracy	Maximum error (m)
NP-KF1 $\gamma = 5$	0.72	0.52	0.74	2.30
NP-KF1 $\gamma = 4$	0.66	0.42	0.76	1.79
NP-KF1 $\gamma = 3$	0.64	0.41	0.78	1.79
NP-KF1 $\gamma = 2$	0.37	0.33	0.92	1.45
RAPS1	0.35	0.31	0.95	1.41
NP-KF2 $\gamma = 5$	0.37	0.32	0.96	1.45
NP-KF2 $\gamma = 4$	0.37	0.32	0.96	1.45
NP-KF2 $\gamma = 3$	0.37	0.32	0.96	1.45
NP-KF2 $\gamma = 2$	0.33	0.31	0.96	1.45
RAPS2	0.33	0.31	0.96	1.45